Supporting Information

Low-temperature topotactic oxidation using solid-state oxidant Zr-doped CeO_2

Masanagi Abe,[a] Hideyuki Kawasoko[a] and Tomoteru Fukumura*[a,b]

[a]Department of Chemistry, Graduate School of Science, Tohoku University, Sendai 980-8578, Japan

[b]Advanced Institute for Materials Research and Core Research Cluster, Tohoku University, Sendai 980-8577, Japan

* tomoteru.fukumura.e4@tohoku.ac.jp

Table S1 Summary of crystal structural data and superconducting transition temperature (T_c) for Y_2O_2Bi before and after topotactic oxidation (TO) with X_{CZO} = 0 at various temperatures (R_{wp}: R-factor, R_e: expected R-factor, S: goodness-of-fit indicator).

	Before TO	X_{CZO} = 0							
		100 °C	200 °C	300 °C	400 °C	500 °C	600 °C	700 °C	800 °C
a (Å)	3.87248(11)	3.87191(8)	3.87094(6)	3.87123(7)	3.87134(7)	3.86999(6)	3.87147(6)	3.87036(8)	3.87201(10)
c (Å)	13.2504(6)	13.2561(4)	13.2499(4)	13.2524(4)	13.2499(4)	13.2453(4)	13.2567(4)	13.2537(5)	13.2560(6)
V (Å^3)	198.704(12)	198.732(8)	198.539(7)	198.606(7)	198.579(8)	198.373(7)	198.695(7)	198.538(8)	198.799(11)
Y z	0.3323(3)	0.3330(2)	0.3327(2)	0.3328(2)	0.3324(3)	0.3326(2)	0.3324(2)	0.3327(3)	0.3318(3)
R_{wp}	3.165	4.168	2.862	2.817	2.776	2.922	2.805	3.319	3.212
R_e	1.789	2.074	2.162	1.955	1.805	1.956	1.839	1.989	1.785
S	1.7686	2.0098	1.5520	1.4408	1.5380	1.4940	1.5248	1.6684	1.7988
c/a	3.4217(2)	3.4237(1)	3.4229(1)	3.4233(1)	3.4226(1)	3.4226(1)	3.4242(1)	3.4244(1)	3.4235(2)
T_c (K)	–	–	–	2.00	1.90	2.07	2.10	2.00	–
Y_2O_2Bi (mol%)	95.3	>99	93.7	94.5	92.3	93.6	94.8	95.3	89.7
Bi (mol%)	4.7	–	6.3	5.5	7.7	6.4	5.2	4.7	10.3
Y_2O_3 (mol%)	–	–	–	–	–	–	–	–	–

Table S2 Summary of crystal structural data and T_c for Y_2O_2Bi after topotactic oxidation with X_{CZO} =1 at various temperatures (R_{wp}: R-factor, R_e: expected R-factor, S: goodness-of-fit indicator)

	$X_{CZO} = 1$							
	100 °C	200 °C	300 °C	400 °C	500 °C	600 °C	700 °C	800 °C
a (Å)	3.87332(7)	3.87163(7)	3.87103(7)	3.87139(10)	3.87033(7)	3.87160(7)	3.87018(6)	3.87108(9)
c (Å)	13.2602(4)	13.2522(4)	13.2496(4)	13.2594(5)	13.2505(4)	13.2580(4)	13.2550(4)	13.2526(5)
V (Å^3)	198.938(7)	198.645(8)	198.543(8)	198.727(11)	198.485(8)	198.728(8)	198.537(7)	198.593(10)
Y z	0.3327(2)	0.3326(2)	0.3329(2)	0.3323(3)	0.3326(3)	0.3322(3)	0.3328(2)	0.3324(3)
R_{wp}	3.898	3.095	2.789	3.013	2.787	3.088	2.995	3.321
R_e	2.079	1.811	1.971	1.770	2.048	1.821	2.094	1.815
S	1.8755	1.7088	1.4150	1.7018	1.3609	1.6955	1.4306	1.8302
c/a	3.4235(1)	3.4299(1)	3.4228(1)	3.4250(2)	3.4236(1)	3.4244(1)	3.4249(1)	3.4235(2)
T_c (K)	–	2.22	2.22	2.20	2.13	2.16	–	–
Y_2O_2Bi (mol%)	>99	92.2	94.4	90.3	86.1	74.4	74.9	73.2
Bi (mol%)	–	7.8	5.6	9.7	7.2	15.9	15.9	20.6
Y_2O_3 (mol%)	–	–	–	–	6.7	9.7	9.7	6.2

Table S3 Summary of crystal structural data and T_c for Y_2O_2Bi after topotactic oxidation with X_{CZO} =10, 50 at various temperatures (R_{wp}: R-factor, R_e: expected R-factor, S: goodness-of-fit indicator).

	X_{CZO} = 10							X_{CZO} = 50
	100 °C	200 °C	200 °C*	400 °C	600 °C	800 °C	800 °C*	200 °C
a (Å)	3.87313(8)	3.87269(7)	3.87386(7)	3.87109(8)	3.87142(10)	3.87135(13)	3.87357(11)	3.87003(9)
c (Å)	13.2629(4)	13.2658(4)	13.2638(4)	13.2613(4)	13.2751(5)	13.2665(6)	13.2690(6)	13.2668(6)
V (Å^3)	198.959(7)	198.959(8)	199.047(8)	198.726(9)	198.965(10)	198.830(13)	199.100(12)	198.729(10)
Y z	0.3325(2)	0.3333(2)	0.3325(2)	0.3322(3)	0.3325(3)	0.3326(4)	0.3312(3)	0.3329(3)
R_{wp}	4.170	3.229	3.291	3.410	4.086	4.085	4.344	3.629
R_e	2.071	2.439	1.525	2.053	2.002	1.975	1.494	2.123
S	2.0132	1.5776	2.1579	1.6607	2.0410	2.0687	2.9079	1.7096
c/a	3.4243(1)	3.4255(1)	3.4239(1)	3.4257(1)	3.4290(2)	3.4268(2)	3.4255(2)	3.4281(2)
T_c (K)	–	2.30	2.18	2.21	2.20	2.16	2.11	2.30
Y_2O_2Bi (mol%)	>99	93.4	92.5	80.3	74.8	72.0	66.8	86.9
Bi (mol%)	–	4.2	6.4	7.3	12.6	6.0	6.4	11.0
YBi (mol%)	–	2.4	1.1	–	–	–	–	2.1
Y_2O_3 (mol%)	–	–	–	12.4	12.5	22.0	26.8	–

* Y_2O_2Bi for magnetic susceptibility measurements in Fig S6, where the T_c was determined by the onset of Meissner effect.

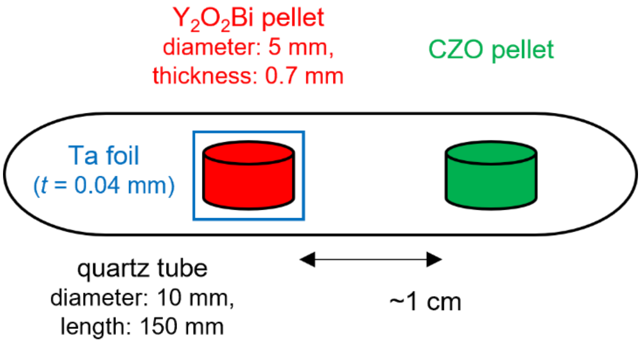

Fig. S1 Schematic illustration inside the quartz tube for the topotactic oxidation.

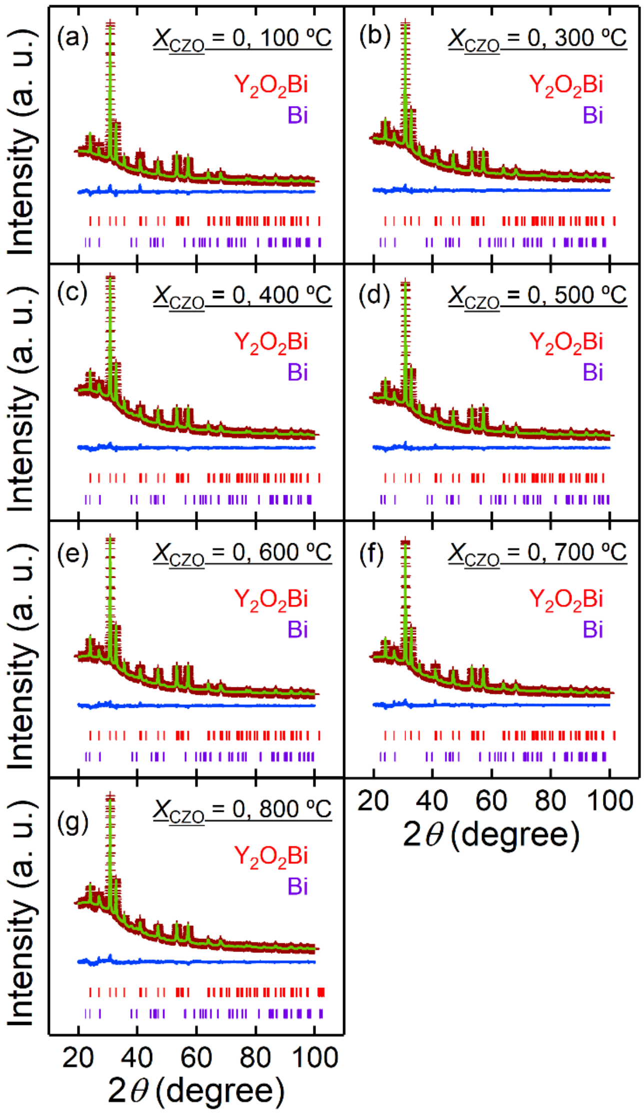

Fig. S2 XRD patterns and Rietveld analysis of Y_2O_2Bi after topotactic oxidation with X_{CZO} = 0 at (a) 100 °C, (b) 300 °C, (c) 400 °C, (d) 500 °C, (e) 600 °C, (f) 700 °C, and (g) 800 °C.

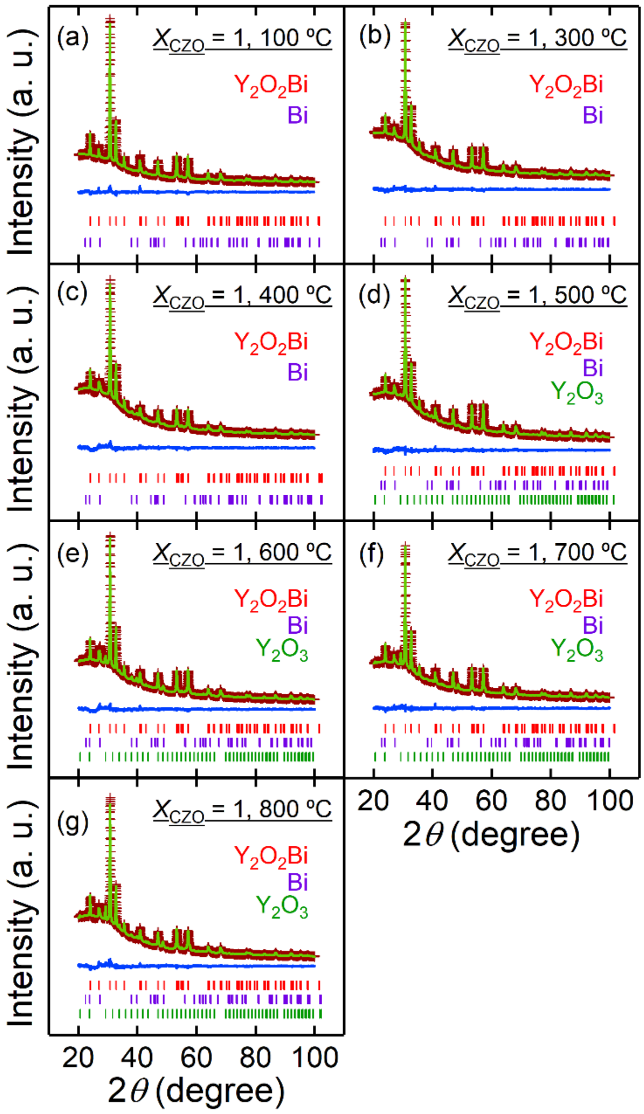

Fig. S3 XRD patterns and Rietveld analysis of Y_2O_2Bi samples after topotactic oxidation with X_{CZO} = 1 at (a) 100 °C, (b) 300 °C, (c) 400 °C, (d) 500 °C, (e) 600 °C, (f) 700 °C, and (g) 800 °C.

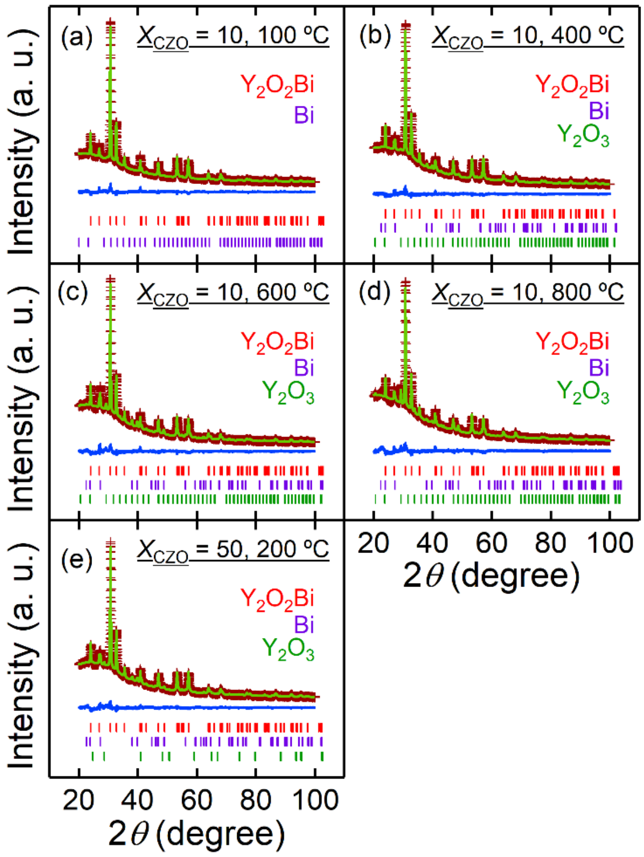

Fig. S4 XRD patterns and Rietveld analysis of Y_2O_2Bi samples after topotactic oxidation with X_{CZO} = 10 at (a) 100 °C, (b) 400 °C, (c) 600 °C, (d) 800 °C, and (e) with CZO (50 mol) at 200 °C.

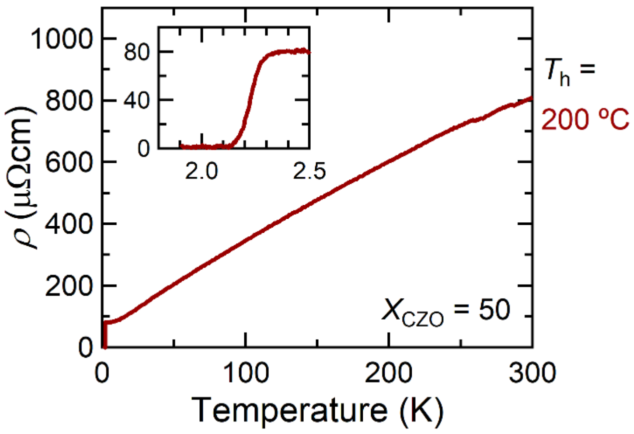

Fig. S5 Temperature dependence of resistivity for Y_2O_2Bi after topotactic oxidation with X_{CZO} = 50 at 200 °C.

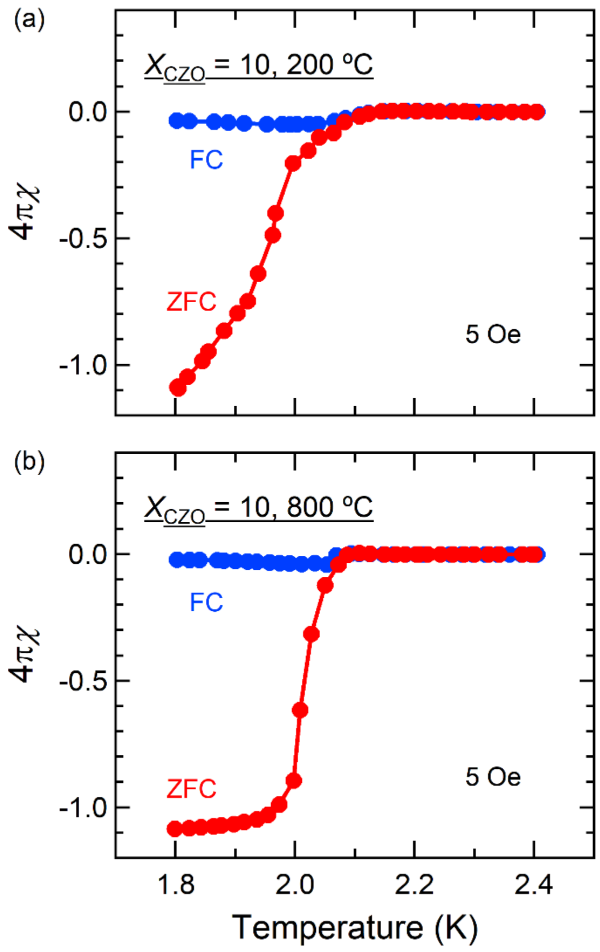

Fig. S6 Temperature dependence of magnetic susceptibility for Y_2O_2Bi after topotactic oxidation with X_{CZO} = 10 at T_h = (a) 200 °C and (b) 800 °C. ZFC and FC denote zero-field cooling and field cooling, respectively. The superconducting volume fraction was 109% and 108% at 1.8 K for (a) and (b), respectively.